THE JOURNAL OF BIOLOGICAL CHEMISTRY VOL. 284, NO. 44, pp. 30218–30229, October 30, 2009

Adipose Triglyceride Lipase Deficiency Causes Tissue-specific Changes in Insulin Signaling*

Received for publication, July 27, 2009, and in revised form, August 26, 2009 Published, JBC Papers in Press, August 31, 2009, DOI 10.1074/jbc.M109.047787

Petra C. Kienesberger[‡§1], Daeho Lee[§¶], Thomas Pulinilkunnil[‖], Daniel S. Brenner[§], Lingzhi Cai[**], Christoph Magnes[‡‡], Harald C. Koefeler[§§], Ingo E. Streith[‡], Gerald N. Rechberger[‡], Guenter Haemmerle[‡], Jeffrey S. Flier[§], Rudolf Zechner[‡], Young-Bum Kim[§2], and Erin E. Kershaw[§3]**

From the [‡]Institute of Molecular Biosciences, University of Graz, A-8010 Graz, Austria, [§]Division of Endocrinology and Metabolism, Department of Medicine, Beth Israel Deaconess Medical Center and Harvard Medical School, Boston, Massachusetts 02215, [¶]Department of Internal Medicine, Jeju National University College of Medicine, Jeju 690-756, Republic of Korea, [‖]Cardiovascular Research Centre, Department of Pediatrics, Faculty of Medicine and Dentistry, University of Alberta, Edmonton, Alberta T6G 2S2, Canada, [**]Division of Endocrinology and Metabolism, Department of Medicine, University of Pittsburgh, Pittsburgh, Pennsylvania 15261, [‡‡]Institute of Medical Technologies and Health Management, Joanneum Research, A-8036 Graz, Austria, and [§§]Core Facility for Mass Spectrometry/Lipidomics, Center for Medical Research, Medical University of Graz, A-8010 Graz, Austria

Triacylglycerol accumulation in insulin target tissues is associated with insulin resistance. Paradoxically, mice with global targeted deletion of adipose triglyceride lipase (ATGL), the rate-limiting enzyme in triacylglycerol hydrolysis, display improved glucose tolerance and insulin sensitivity despite triacylglycerol accumulation in multiple tissues. To determine the molecular mechanisms for this phenotype, ATGL-deficient ($ATGL^{-/-}$) and wild-type mice were injected with saline or insulin (10 units/kg, intraperitoneally), and then phosphorylation and activities of key insulin-signaling proteins were determined in insulin target tissues (liver, adipose tissue, and muscle). Insulin signaling and/or glucose transport was also evaluated in isolated adipocytes and skeletal muscle *ex vivo*. In $ATGL^{-/-}$ mice, insulin-stimulated phosphatidylinositol 3-kinase and Akt activities as well as phosphorylation of critical residues of IRS1 (Tyr(P)-612) and Akt (Ser(P)-473) were increased in skeletal muscle *in vivo*. Insulin-stimulated phosphatidylinositol 3-kinase activity and total insulin receptor and insulin receptor substrate 1, but not other parameters, were also increased in white adipose tissue *in vivo*. In contrast, *in vivo* measures of insulin signaling were decreased in brown adipose tissue and liver. Interestingly, the enhanced components of insulin signaling identified in skeletal muscle and white adipose tissue *in vivo* and their expected downstream effects on glucose transport were not present *ex vivo*. ATGL deficiency altered intramyocellular lipids as well as serum factors known to influence insulin sensitivity. Thus, skeletal muscle, rather than other tissues, primarily contributes to enhanced insulin sensitivity in $ATGL^{-/-}$ mice *in vivo* despite triacylglycerol accumulation, and both local and systemic factors contribute to tissue-specific effects of global ATGL deficiency on insulin action.

Triacylglycerols (TAGs)[4] are the predominant form of energy storage in animals. The ability to store and release this energy in response to variable energy availability requires a carefully regulated balance between TAG synthesis and hydrolysis. In the setting of chronic energy excess, however, TAGs and other lipid metabolites accumulate in adipose tissue as well as in metabolically relevant non-adipose tissues where they have been proposed to contribute to cellular dysfunction via a process known as lipotoxicity (1–3). Indeed, intracellular TAG accumulation has been repeatedly associated with metabolic dysfunction, a relationship that is particularly strong for insulin resistance (1–3). Despite this strong association, however, intracellular TAG accumulation is not always associated with insulin resistance (4) and may even be associated with insulin sensitivity, as is the case with highly trained endurance athletes (the so-called "athlete paradox") (5). Thus, the contribution of intracellular TAGs and TAG metabolism *per se* to lipotoxicity remains controversial. What is clear is that lipid-induced insulin resistance is a major risk factor for morbidity and mortality from a variety of causes, including overt diabetes mellitus, non-alcoholic fatty liver disease, and cardiovascular disease. Hence, understanding the mechanisms by which dysregulated TAG metabolism contributes to steatosis, lipotoxicity, and insulin resistance is essential to understanding and treating these increasingly prevalent disorders.

* This work was supported, in whole or in part, by National Institutes of Health Grants K08-DK065833 and R03-DK077697 (to E. E. K.), R37-DK028082 (to J. S. F.), DK043051 (to Y. B. K.), and P30-DK57521 (to the Beth Israel Deaconess Medical Center Metabolic Physiology Core Facility). This work was also supported by Austrian Ministry of Science and Research GEN-AU Grant GOLD-Genomics of Lipid-associated Disorders (to R. Z.), F30 (SFB LIPOTOX) (to R. Z.), Wittgenstein Award Z136 (to R. Z.), Austrian Science Foundation Grant W901 DK (to R. Z. and P. C. K.), and American Diabetes Association Grant 1-09-RA-87 (to Y. B. K.).

[1] Present address: Cardiovascular Research Centre, Dept. of Pediatrics, Faculty of Medicine and Dentistry, University of Alberta, Edmonton, Alberta T6G2S2, Canada.

[2] To whom correspondence may be addressed: 330 Brookline Ave., CLS-736, Boston, MA 02215. Tel.: 617-735-3216; Fax: 617-735-3233; E-mail: ykim2@bidmc.harvard.edu.

[3] To whom correspondence may be addressed: 200 Lothrop St., E1140 Thomas E. Starzl Biomedical Science Tower, Pittsburgh, PA 15261. Tel.: 412-648-8454; Fax: 412-648-3290; E-mail: kershawe@pitt.edu.

[4] The abbreviations used are: TAG, triacylglycerol; ATGL, adipose triglyceride lipase; BAT, brown adipose tissue; DAG, diacylglycerol; FA, fatty acid or fatty acyl; FA-CoA, fatty acyl-CoA; IR, insulin receptor; IRS, insulin receptor substrate; PI3K, phosphatidylinositol 3-kinase; WAT, white adipose tissue; NEFA, nonesterified fatty acid; EDL, extensor digitorum longus; GTT, glucose tolerance test; ITT, insulin tolerance test; ANOVA, analysis of variance; MS, mass spectrometry; GAPDH, glyceraldehyde-3-phosphate dehydrogenase; WT, wild type; HSL, hormone-sensitive lipase.

Although no mechanistic data have been identified directly linking intracellular TAGs *per se* to insulin resistance, lipotoxicity may occur when the capacity of the lipid droplets to effectively store TAGs is exceeded. Several other lipid metabolites that are products of TAG hydrolysis (*i.e.* diacylglyerols (DAGs), fatty acids (FAs), fatty acyl-CoAs (FA-CoAs), and ceramides) have been shown to directly or indirectly interfere with insulin signaling and glucose transport via a variety of mechanisms (6–9). Under normal physiological circumstances, insulin binds to the insulin receptor (IR), thereby triggering its intrinsic protein-tyrosine kinase activity. The subsequent autophosphorylation of several IR tyrosine residues promotes the recruitment and tyrosine phosphorylation of IR substrates (IRSs) followed by activation of phosphatidylinositol 3-kinase (PI3K) and Akt, which in turn promote the pleiotrophic downstream effects of insulin. The above lipid metabolites have been shown to increase serine/threonine phosphorylation and decrease tyrosine phosphorylation of IRS1, decrease serine/threonine phosphorylation of Akt, decrease IRS1-associated PI3K activity and Akt activity, and decrease Glut4 translocation (6–9). Possible mechanisms by which these lipid metabolites may influence glucose homeostasis and insulin action include competition for substrate oxidation, interference with cellular energy sensing, regulation of gene expression, promotion of oxidative stress and mitochondrial dysfunction, and activation of inflammatory and apoptotic pathways (6–9). However, most studies evaluating the role of lipotoxicity in insulin resistance have focused on cellular lipid uptake or oxidation, both of which produce unidirectional changes in intracellular TAGs and other intracellular lipid metabolites and hence do not adequately address the role of intracellular TAGs and TAG metabolism *per se* to this process.

Understanding the role of TAG metabolism in lipotoxicity and insulin resistance has been further complicated by the fact that the rate-limiting enzyme for TAG hydrolysis, adipose triglyceride lipase (ATGL), has only recently been identified (10–12). ATGL has been most extensively studied in adipose tissue where it mediates the hydrolysis of long chain fatty acyl TAGs (10). ATGL is also expressed in other tissues, including liver, muscle, and pancreas (13), where its contribution to tissue-specific and systemic metabolism is less well understood. Mice with global targeted deletion of ATGL ($ATGL^{-/-}$ mice) have severe defects in TAG hydrolysis, leading to TAG accumulation in virtually all tissues (14). Surprisingly, despite increased adiposity and "ectopic" TAG accumulation, which are characteristically associated with insulin resistance, $ATGL^{-/-}$ mice paradoxically exhibit enhanced glucose tolerance and insulin sensitivity (14). This finding has largely been attributed to the effect of reduced systemic FA delivery on energy substrate availability (14). However, the contribution of altered tissue-specific insulin action to this phenotype has not been evaluated.

$ATGL^{-/-}$ mice represent a unique model for examining the contribution of intracellular TAG accumulation to glucose homeostasis and insulin action because intracellular TAG accumulation is dissociated from systemic FA delivery, and presumably also from the production/accumulation of other intracellular lipid metabolites. In addition, $ATGL^{-/-}$ mice differ from the other models in which increased adiposity is paradoxically associated with insulin sensitivity in that enhanced expansion of adipose tissue mass and reduced systemic FA delivery do not protect against ectopic lipid deposition in $ATGL^{-/-}$ mice (15, 16). The aims of this study were to evaluate the mechanisms by which impaired TAG hydrolysis and intracellular TAG accumulation because of global ATGL deficiency promote whole-body glucose tolerance and insulin sensitivity and to define the contribution of tissue-specific changes in insulin action to this phenotype. Here we demonstrate that global ATGL deficiency in mice not only reduces energy substrate availability but also produces tissue-specific changes in insulin action.

EXPERIMENTAL PROCEDURES

Animals—Mice were housed under standard conditions at 25 °C with a 14:10 h light/dark cycle with *ad libitum* access to water and standard chow diet (Harlan Teklad RD 8664). Mice were handled in accordance with guidelines established by the National Institutes of Health. Experimental procedures were approved by the Institutional Animal Care and Use Committee. $ATGL^{-/-}$ mice were generated on a mixed genetic background (50% C57BL/6 and 50% 129/Ola) as described (14). The targeted ATGL allele was then backcrossed onto the obesogenic/diabetogenic C57BL/6 background strain for >10 generations. Experimental mice were generated by breeding $ATGL^{+/-}$ or $ATGL^{-/-}$ males to $ATGL^{+/-}$ females. Because $ATGL^{-/-}$ mice develop premature morbidity and mortality as well as profound hypothermia and hypometabolism (torpor) in response to prolonged fasting (14), studies were performed under more physiological conditions (short term fasting of 6–8 h) using mice less than 14 weeks of age.

Body Composition and Metabolic Measurements—Body composition was determined in awake mice using EchoMRI (Echo Medical Systems). Plasma glucose was measured using a One-touch FastTake glucometer (Lifescan). For insulin and glucose tolerance tests (ITT and GTT, respectively), awake mice were injected intraperitoneally with human insulin (HumulinR; Lilly) at 0.75 units per kg of body weight (ITT) or with 20% D-glucose at 1.5 g per kg of body weight (GTT) followed by blood sampling at the times indicated.

Analysis of Serum Insulin, Adipokines, and Lipids—Serum insulin was determined using the rat insulin enzyme-linked immunosorbent assay kit (Crystal Chem). Serum resistin and adiponectin were determined using Lincoplex enzyme-linked immunosorbent assay kits (Millipore). Serum retinol-binding protein 4 (RBP4) was determined using anti-human RBP4 polyclonal antibody (Dako) as described (17). Serum nonesterified fatty acids (NEFAs) and TAGs were determined using the HR Series NEFA-HR(2) colorimetric assay (Wako Chemical Industries) and the Triglyceride Liquicolor colorimetric assay (Stan-Bio Laboratory), respectively.

Liver Glycogen Determination—Liver glycogen was assayed according to Adamo and Graham (18) with modifications. Liver was homogenized on ice in 0.03 M HCl per 100 mg of tissue. Aliquots of 500 μl were mixed with equal volumes of 2 M HCl and then neutralized by adding 500 μl of 2 M NaOH for the determination of free glucose or subjected to continued incubation for 2 h at 99 °C to determine total glucose. Samples were then centrifuged for 30 min at 14,000 × *g*, 4 °C, and glucose concentration in the supernatant was measured using Thermo Trace glucose oxidase

reagent (Thermo Electron). Glycogen-derived glucose was calculated by subtracting free from total glucose.

Insulin Signaling Studies—For insulin signaling studies *in vivo*, 6-h fasted mice were injected intraperitoneally with insulin at 10 units per kg body weight. Ten min thereafter, mice were sacrificed by cervical dislocation, and tissues were collected. For muscle insulin signaling studies *ex vivo*, soleus muscles were rapidly dissected from 6-h fasted mice after sacrifice by cervical dislocation and preincubated for 30 min in pre-gassed (95% O_2, 5% CO_2) Krebs-Henseleit bicarbonate buffer, pH 7.4, containing 5 mM Hepes (KHB + Hepes) at 35 °C. Contralateral muscles were then incubated for 10 min in buffer with or without 33 nM insulin. Muscles were removed, blotted dry, snap-frozen in liquid nitrogen, and stored at −80 °C until processing.

Immunoblotting Analysis—Tissues were homogenized in ice-cold lysis buffer (20 mM Tris-HCl, pH 7.4, 5 mM EDTA, 10 mM $Na_4P_2O_7$, 100 mM NaF, 1% Nonidet P-40, 2 mM Na_3VO_4, 1 mM phenylmethylsulfonyl fluoride, 14 μM leupeptin, 1 μM aprotinin). Lysates were centrifuged at 14,000 × *g* for 30 min at 4 °C, and supernatants were stored at −80 °C until analysis. Lysate protein was resolved by SDS-PAGE (Criterion, Bio-Rad) and transferred to nitrocellulose membranes (Whatman Protran, Fisher). Phosphorylated and total proteins were identified by immunoblotting using the following primary antibodies: anti-pIR (Tyr(P)-1162/ Tyr(P)-1163) polyclonal, anti-pIR (Tyr(P)-972) polyclonal, and anti-pIRS1 (Tyr(P)-612) polyclonal (Invitrogen); anti-IRβ polyclonal and anti-IRα polyclonal (Santa Cruz Biotechnology); anti-IRS1 polyclonal, anti-pAkt (Ser(P)-473) monoclonal, and anti-Akt polyclonal (Millipore); anti-pAkt (Thr(P)-308) monoclonal (Cell Signaling); anti-GAPDH polyclonal (Imgenex); and anti-Ran GTPase monoclonal (BD Biosciences). Immunoblots were developed using a Western blot chemiluminescence reagent (PerkinElmer Life Sciences). Densitometric analysis was performed using ImageJ software (National Institutes of Health).

PI3K and Akt Activity Assays—For PI3K activity, tissue lysates (liver and gastrocnemius muscle, 500 μg of protein; white and brown adipose, 300 μg; soleus muscle, 100 μg) were subjected to immunoprecipitation overnight at 4 °C with 4 μg of polyclonal anti-IRS1 antibody (Millipore) or 2 μl of polyclonal anti-IRS2 (gift from Morris White, Joslin Diabetes Center, Boston) coupled to protein A-Sepharose beads (Sigma). For Akt activity, tissue lysates were subjected to immunoprecipitation for 4 h at 4 °C with 4 μg of anti-Akt monoclonal antibody (Millipore) coupled to protein G-Sepharose beads (GE Healthcare). The immune complexes were washed, and PI3K and Akt activities were determined as described previously (19).

Muscle 2-[^{3}H]Deoxyglucose Transport ex Vivo—Glucose transport into muscle *ex vivo* was determined according to Zisman *et al.* (20) with modifications. Soleus and extensor digitorum longus (EDL) muscles were rapidly dissected from 6-h fasted mice after sacrifice by cervical dislocation. Muscles were then preincubated for 1 h in KHB + Hepes supplemented with 10 mM D-glucose at 35 °C, and rinsed by incubation for 10 min in KHB + Hepes supplemented with 10 mM D-mannitol. Glucose transport was assessed by subsequent incubation in KHB + Hepes containing 1 mM 2-deoxyglucose, 9 mM mannitol, 1.5 μCi/ml 2-deoxy-D-[1,2-^{3}H]glucose (American Radiolabeled Chemicals), and 0.3 μCi/ml D-[1-^{14}C]mannitol (American Radiolabeled Chemicals) for 20 min at 29 °C. To determine basal and insulin-stimulated glucose transport in contralateral muscles, all buffers were pre-gassed with 95% O_2, 5% CO_2 and supplemented with equal volumes of saline or 33 nM insulin, respectively. After the final incubation, muscles were removed, blotted dry, trimmed, and snap-frozen in liquid nitrogen. Later, the muscles were weighed and digested for 30 min in 300 μl of 1 M NaOH at 65 °C and centrifuged at 13,000 × *g* for 10 min at ambient temperature. Radioactivity in the supernatant was determined by liquid scintillation counting for dual labels, and glucose transport into myotubes was calculated.

[^{14}C]Glucose Transport into Isolated Adipocytes—Glucose uptake in isolated adipocytes was determined using conditions in which glucose uptake is directly proportional to transport as described previously (21). Briefly, adipocytes were isolated from epididymal fat pads by collagenase (1 mg/ml) digestion. A fraction of isolated adipocytes was used to determine the average cell number and volume (μg of lipid/cell) (22). The remaining adipocytes were incubated at 37 °C with constant agitation in a 10% (v/v) suspension of Krebs-Ringer bicarbonate buffer, pH 7.4, containing 20 mM Hepes, 2.5% bovine serum albumin (fraction V), and 200 nM adenosine for 30 min with 0, 0.2, 0.3, 0.4, 0.6, 1, 5, or 100 nM insulin. Glucose uptake into adipocytes was assayed by the subsequent incubation with 3 mM [U-^{14}C]glucose (286 mCi/mmol; Amersham Biosciences) for 30 min. The reaction was terminated by brief centrifugation over dinonyl phthalate oil, and the radioactivity in the cell layer (supernatant) was determined by liquid scintillation counting.

Muscle Lipid Analysis—Oil Red O staining of neutral lipids in skeletal muscle was performed as described (23). For biochemical analysis of TAGs, DAGs, and ceramides, soleus muscle lipids were extracted using the method of Folch *et al.* (24). The organic solvent was evaporated under a stream of nitrogen, and lipid extracts were stored at −20 °C until processing. For TAG analysis, lipids were resuspended in ice-cold 1% Triton X-100 by sonication. TAG concentration was determined using a colorimetric kit assay (Thermo Trace; Thermo Scientific). To determine ceramide concentrations, lipid extracts were redissolved in 400 μl of $CHCl_3$/MetOH/H_2O (16:16:5, v/v), followed by addition of 400 μl of 0.2 N methanolic NaOH and incubation for 45 min at ambient temperature under constant shaking. Thereafter, 400 μl of 0.5 M EDTA and 150 μl of 1 N acetic acid were added (25). After lipid extraction using $CHCl_3$, the organic solvent was evaporated under a stream of nitrogen, and lipids were redissolved in acetonitrile/isopropyl alcohol (5:2, v/v) containing 1% NH_4 acetate and 0.1% formic acid for high pressure liquid chromatography-MS/MS analysis. Ceramides were analyzed by tandem mass spectroscopy using a Quantum TSQ (Thermo Electron) coupled to the Accela UPLC system (Thermo Electron). For DAG analysis, lipid extracts were directly redissolved in acetonitrile/isopropyl alcohol (5:2, v/v) containing 1% NH_4 acetate and 0.1% formic acid and analyzed using the Accela UPLC-LTQ-FT MS system (Thermo Electron). FA-CoAs were determined by on-line SPE-LC-MS according to the method of Magnes *et al.* (26).

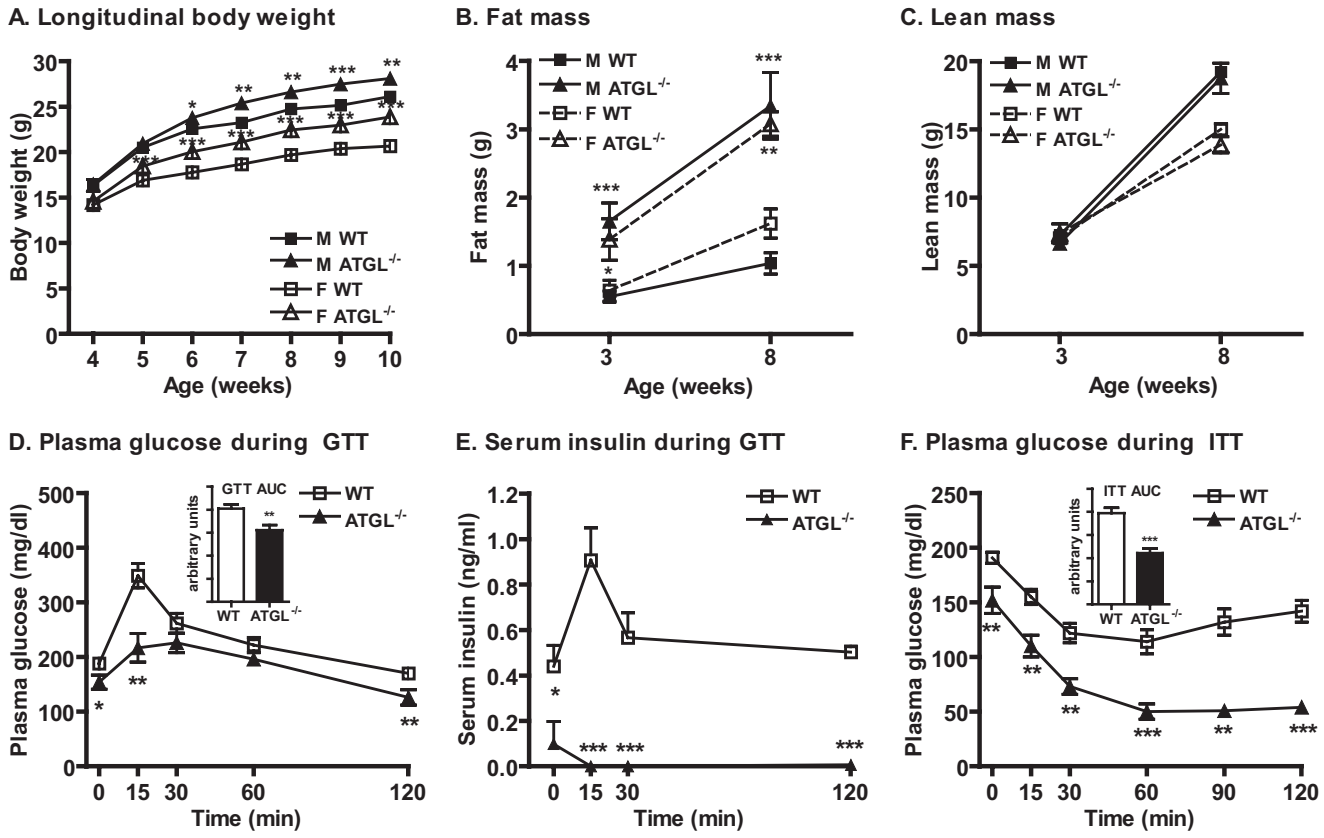

FIGURE 1. **Body weight, body composition, glucose tolerance, and insulin sensitivity.** *A,* body weight of male (*M*) and female (*F*) WT and ATGL$^{-/-}$ mice ($n = 16–41$ per group). *B,* total body fat mass, and *C,* lean mass of WT and ATGL$^{-/-}$ mice as assessed by EchoMRI ($n = 3–17$ per group). *D,* GTT, plasma glucose in 7–8-h fasted male mice at 8–10 weeks of age following intraperitoneal administration of 1.5 g of glucose/kg of body weight ($n = 8–18$ per group). *E,* serum insulin following administration of 1.5 g of glucose/kg of body weight in a separate cohort of 7–8 week-old mice of mixed gender ($n = 4–5$ per group). Experimental conditions and blood glucose curves were comparable with the GTT shown in *D*. *F*, ITT, plasma glucose in 7–8-h fasted male mice at 7–9 weeks of age following intraperitoneal administration of 0.75 units of insulin/kg of body weight ($n = 8–18$ per group). For both ITT and GTT, the areas under the curve are shown (*D* and *F*, *insets*). Data are expressed as mean ± S.E. *, $p < 0.05$; **, $p < 0.01$; ***, $p < 0.001$ for effect of genotype as determined by unpaired two-tailed Student's *t* test.

RNA Extraction, Reverse Transcription, and Gene Expression Analysis—Total RNA was extracted from homogenized tissues using RNeasy lipid tissue mini kit with on-column DNase treatment (Qiagen). Reverse transcription of 1 μg of total RNA was performed using random decamers (RETROscript kit, Ambion, Inc.). Gene expression was determined by quantitative PCR (7300 real time PCR system, Applied Biosystems). Reactions were performed in triplicate in 25 μl containing 2.5 μl of 1:100 diluted cDNA, 1× Taqman Universal PCR master mix (Applied Biosystems), and gene-specific primer-probe sets (Taqman Gene Expression Assays, Applied Biosystems). Reactions were run at 95 °C for 10 min followed by 40 cycles of 95 °C for 15 s and 60 °C for 1 min. Gene expression was determined by the standard curve method and normalized to expression of cyclophilin as reference gene (forward 5′-GGTAGGAGAGCACCAAGACAGA, reverse 5′-GCCGGAGTCGACAATAGATAG, and probe 5′-AGCCGGGACAAGCCACTAGAAGGAT). Appropriate analysis was performed to determine that expression of control genes was unchanged under the experimental conditions described. Accuracy of RNA quantification was optimized by DNase treatment of samples, use of gene-specific primer-probe sets that span intron-exon boundaries, and verification of lack of amplification in no-reverse transcriptase and no-template controls.

Statistical Analysis—Results are expressed as means ± S.E. Comparisons between groups were made by unpaired two-tailed Student's *t* test or one-way analysis of variance (ANOVA), as appropriate. Where differences were found by ANOVA, *post hoc* analysis was performed using Bonferroni's multiple comparison test. For glucose transport into isolated adipocytes, nonlinear regression was used to generate a best fit concentration-response curve using a variable slope sigmoidal (Hill) equation with no constraints. For all analyses, *p* values of <0.05 were considered statistically significant.

RESULTS

ATGL$^{-/-}$ Mice on a Pure C57BL/6 Background Have Improved Glucose Tolerance and Insulin Sensitivity Despite Increased Body Weight and Fat Mass—Because previous observations of improved glucose tolerance and insulin sensitivity were identified in anesthetized ATGL$^{-/-}$ mice on a mixed genetic background (14), we first confirmed the effect of global ATGL deficiency on body weight, body composition, glucose tolerance, and insulin sensitivity in awake mice on a pure C57BL/6 background. ATGL$^{-/-}$ mice on a C57BL/6 background developed significantly increased body weight compared with wild-type (WT) mice as early as 5–6 weeks of age (Fig. 1*A*), much earlier than mice on a mixed background (14).

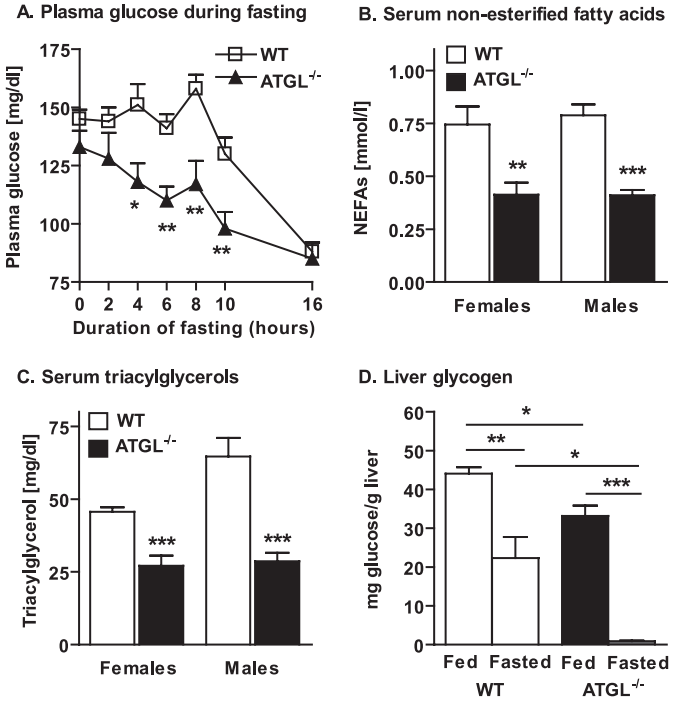

FIGURE 2. **Blood glucose, serum lipids, and liver glycogen.** *A,* plasma glucose during fasting in 6-10-week-old female mice (n = 10–18 per group). *B,* serum NEFAs, and *C,* TAGs in 7–10-week-old mice following a 6-h fast (n = 8 per group). *D,* liver glycogen in *ad libitum*-fed and 6-h-fasted, 7-14-week-old mice of mixed gender (n = 3–4 per group). Data are expressed as means ± S. E. *, $p < 0.05$; **, $p < 0.01$; ***, $p < 0.001$ for effect of genotype or feeding status as determined by unpaired two-tailed Student's t test.

This increase in body weight was entirely due to increased fat mass (Fig. 1*B*) and not due to altered lean mass (Fig. 1*C*). The GTT, which reflects both insulin-independent and -dependent glucose disposal, revealed reduced serum glucose in ATGL$^{-/-}$ mice at 0, 15, and 120 min following glucose injection (Fig. 1*D*) as well as a reduced area under the curve (Fig. 1*D, inset*), consistent with improved glucose tolerance. Interestingly, measurement of serum insulin during the GTT revealed drastically reduced serum insulin at all time points, suggesting that enhanced glucose tolerance in ATGL$^{-/-}$ mice under these conditions is in part due to non-insulin-mediated mechanisms and that ATGL deletion may additionally impair beta cell insulin secretion in response to a glucose challenge (Fig. 1*E*). The ITT, which primarily reflects insulin-mediated glucose disposal, revealed reduced serum glucose in ATGL$^{-/-}$ mice at all time points following intraperitoneal insulin injection (Fig. 1*F*) as well as a reduced area under the curve (Fig. 1*F, inset*), suggesting improved insulin sensitivity. These GTT and ITT results were preserved even after correcting for the initial differences in basal glucose. Similar GTT and ITT results were also obtained in female mice (data not shown).

Reduced Energy Substrate Availability Contributes to Increased Glucose Tolerance in ATGL$^{-/-}$ Mice—To determine the contribution of substrate availability to glucose homeostasis in ATGL$^{-/-}$ mice, we evaluated serum glucose during fasting (0–16 h), hepatic glycogen content during *ad libitum* feeding and following a physiological fast (6 h), and serum lipids following a physiological fast (6 h). Serum glucose concentrations during *ad libitum* feeding and after a prolonged fast did not differ between ATGL$^{-/-}$ and WT mice, consistent with previous reports (Fig. 2*A*) (14). However, although normal serum glucose was maintained in WT mice through 8–10 h of fasting, serum glucose decreased almost immediately in ATGL$^{-/-}$ mice and became significantly lower than WT mice within 4 h of fasting. Not surprisingly, availability of serum lipid substrates (FAs and TAGs) was reduced in ATGL$^{-/-}$ mice following a 6-h fast (Fig. 2, *B* and *C*, respectively). Consistent with enhanced reliance on hepatic glucose production, hepatic glycogen content was reduced in ATGL$^{-/-}$ mice compared with WT mice in both fed and fasted states (Fig. 2*D*). Thus, a reduction in both lipid and carbohydrate substrate contributes to the apparent glucose tolerance in ATGL$^{-/-}$ mice.

Insulin Action Is Impaired in Liver of ATGL$^{-/-}$ Mice—To better understand how global ATGL deficiency contributes to hepatic insulin action and glucose homeostasis in ATGL$^{-/-}$ mice, we evaluated insulin signaling in liver. Insulin-stimulated phosphorylation of the IR at sites Tyr-1162/1163 ($p = 0.06$) and Tyr-972 as well as Akt Ser-473 were not different in ATGL$^{-/-}$ mice (Fig. 3, *A* and *B*). However, insulin-stimulated phosphorylation of IRS1 Tyr-612 and Akt Tyr-308 was decreased in ATGL$^{-/-}$ mice (Fig. 3, *A* and *B*). Expression of total proteins relative to Ran GTPase control gene was unchanged between genotype groups (quantification not shown). Furthermore, although insulin-stimulated IRS1- and IRS2-associated PI3K activities were unchanged (Fig. 3, *C* and *D*), insulin-stimulated Akt activity was decreased in ATGL$^{-/-}$ mice (Fig. 3*E*). These findings suggest that ATGL deficiency contributes to distal impairment in hepatic insulin signaling at the level of Akt, indicating that enhanced insulin signaling in liver does not contribute to whole-body insulin sensitivity in ATGL$^{-/-}$ mice.

Insulin-stimulated Glucose Transport and Insulin Action Are Not Impaired in White Adipose Tissue of ATGL$^{-/-}$ Mice Despite Increased Adipocyte Lipid Content—To better understand how ATGL deficiency influences adipocyte insulin action and glucose homeostasis in ATGL$^{-/-}$ mice, we evaluated insulin signaling in brown and white adipose tissue *in vivo* as well as glucose uptake into isolated white adipocytes *ex vivo*. Evaluation of insulin signaling in brown adipose tissue (BAT) of ATGL$^{-/-}$ mice revealed a similar pattern as was observed for liver, *i.e.* reduced insulin-stimulated phosphorylation of IRS1 at Tyr-612 and Akt activity but no difference in PI3K activity (data not shown), consistent with impaired insulin signaling downstream of the IR. In contrast, in perigonadal white adipose tissue (WAT) *in vivo*, insulin-stimulated phosphorylations of the IR at sites Tyr-1162/1163, IRS1 at Tyr-612, as well as phosphorylation of Akt at Ser-473 were unchanged in ATGL$^{-/-}$ mice (Fig. 4, *A* and *B*). Despite no change in stoichiometric phosphorylation of these sites, total IR and IRS1 protein relative to GAPDH control were increased in ATGL$^{-/-}$ mice (Fig. 4*C*). This increase in total IR an IRS1 was associated with increased insulin-stimulated IRS1-associated PI3K activity (Fig. 4*D*) but not Akt activity (Fig. 4*E*) in ATGL$^{-/-}$ mice. These data suggest that, in contrast to liver and BAT, insulin action was not impaired (and may even be improved) in WAT of ATGL$^{-/-}$ mice.

To further clarify these findings, we next evaluated *ex vivo* glucose transport in isolated white adipocytes. Lipid content

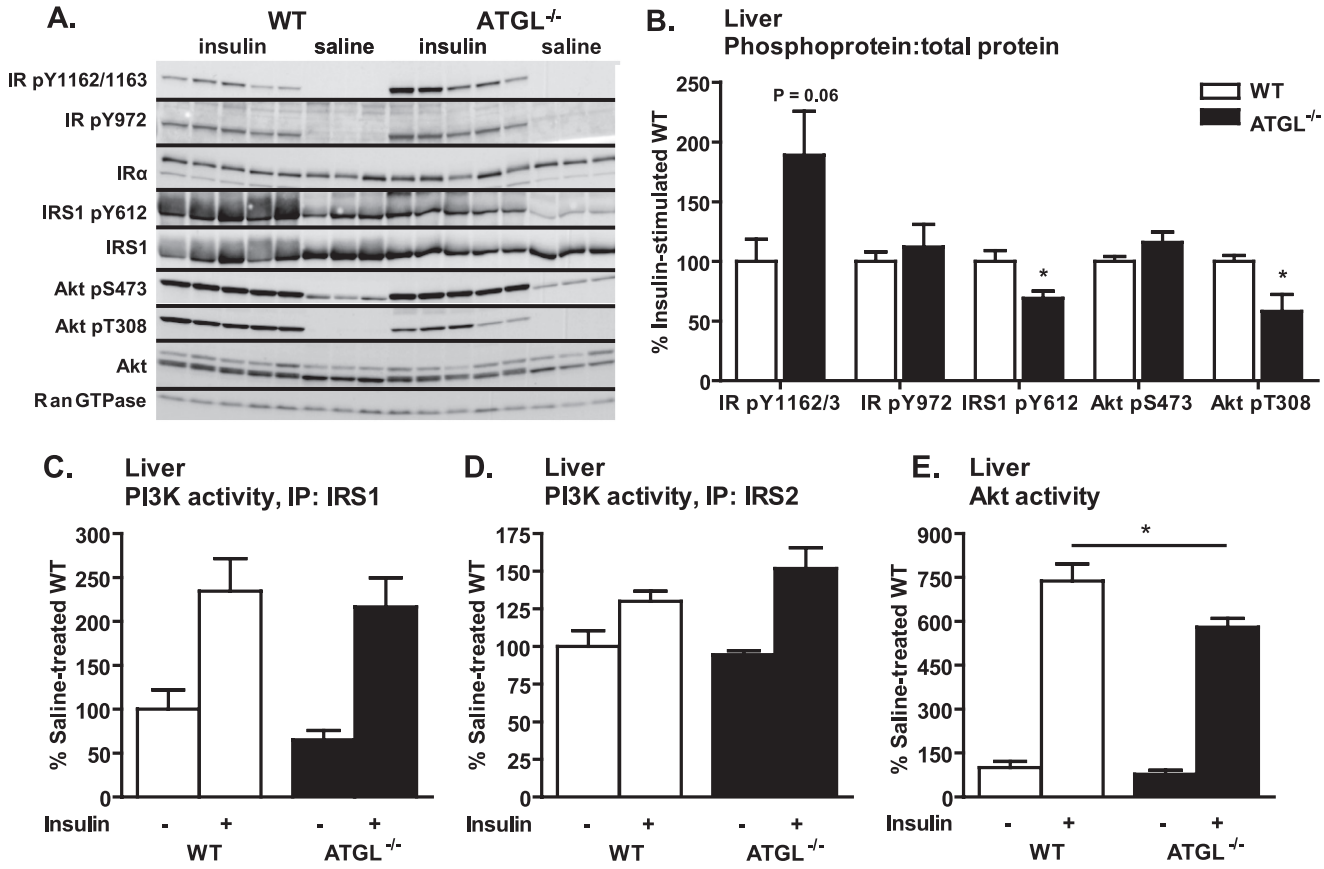

FIGURE 3. **Liver insulin signaling *in vivo*.** Male mice at 10–12 weeks of age were fasted for 6 h, injected intraperitoneally with saline or insulin at 10 units/kg of body weight, and sacrificed 10 min thereafter. *A* and *B*, insulin-stimulated site-specific phosphorylation of IR, IRS1, and Akt as assessed by immunoblotting analysis ($n = 3$–5 per group). For quantification, phosphoproteins were normalized to the corresponding total proteins. Ran GTPase served as loading control. *C*, IRS1-associated PI3K activity; *D*, IRS2-associated PI3K activity; and *E*, Akt activity ($n = 3$–7 per group). *IP*, immunoprecipitation. Data are expressed as mean ± S.E. *, $p < 0.05$ for effect of genotype as determined by unpaired two-tailed Student's *t* test (*B*) or one-way ANOVA (*C*–*E*).

per adipocyte (Fig. 5*A*) and basal glucose transport (Fig. 5*B*) were both increased in ATGL-deficient adipocytes, consistent with previous reports demonstrating a positive correlation between basal glucose transport/cell and adipocyte size (27). However, maximal insulin-stimulated glucose transport rates (V_{max} = 32.45 ± 1.51 amol/min/cell for WT; 32.89 ± 1.77 amol/min/cell for ATGL$^{-/-}$) and the half-maximal effective concentrations for insulin (EC_{50} = 0.2983 nM for WT; EC_{50} = 0.2563 nM for ATGL$^{-/-}$) were not different between groups (Fig. 5*C*), even after correcting for differences in basal glucose transport (Fig. 5*D*). These data suggest that enhanced basal glucose transport into white adipocytes contributes to improved glucose homeostasis in ATGL$^{-/-}$ mice and that insulin-stimulated glucose transport is not impaired despite increased adipocyte lipid content. These data also indicate that the increase in PI3K activity observed *in vivo* does not translate into improved insulin-stimulated glucose transport into adipocytes *ex vivo*.

Insulin Action Is Enhanced in Skeletal Muscle of ATGL$^{-/-}$ Mice in Vivo but Not ex Vivo—To better understand how global ATGL deficiency contributes to skeletal muscle insulin action and glucose homeostasis, we evaluated insulin signaling in skeletal muscle *in vivo* and *ex vivo* as well as glucose transport in skeletal muscle *ex vivo*. We first confirmed that ATGL was comparably expressed in all muscles examined (relative expression of ATGL/cyclophilin by quantitative PCR was 1.00 ± 0.10 for gastrocnemius, 1.12 ± 0.28 for EDL, and 1.15 ± 0.18 for soleus). In skeletal muscle (gastrocnemius) *in vivo*, insulin-stimulated IR Tyr-1162/1163 phosphorylation was unchanged in ATGL$^{-/-}$ mice. However, phosphorylation of IRS1 at Tyr-612 and Akt at Ser-473 was increased, and Akt Thr-308 phosphorylation tended to be increased ($p = 0.06$) (Fig. 6, *A* and *B*) in ATGL$^{-/-}$ mice. Expression of total proteins relative to Ran GTPase control gene was unchanged between genotype groups (quantification not shown). The increase in IRS1 and Akt phosphorylation was associated with increased insulin-stimulated IRS1-associated PI3K and Akt activities (Fig. 6, *C* and *D*, respectively) as well as increased glucose transporter 4 (Glut4) protein expression (Fig. 6*E*) in skeletal muscle of ATGL$^{-/-}$ mice. These findings suggest that increased *in vivo* insulin signaling in skeletal muscle contributes to enhanced whole-body insulin sensitivity in ATGL$^{-/-}$ mice.

Interestingly, evaluation of insulin signaling in skeletal muscle (soleus) *ex vivo* revealed that insulin-stimulated phosphorylation of IR Tyr-1162/1163, Akt Tyr-308, and Akt Ser-473 was unchanged or reduced in ATGL$^{-/-}$ mice (Fig. 7, *A* and *B*). In addition, the previously observed increases in insulin-stimulated IRS1-associated PI3K and Akt activities in skeletal muscle *in vivo* disappeared when insulin stimulation was performed in skeletal muscle *ex vivo* (Fig. 7, *C* and *D*). Furthermore,

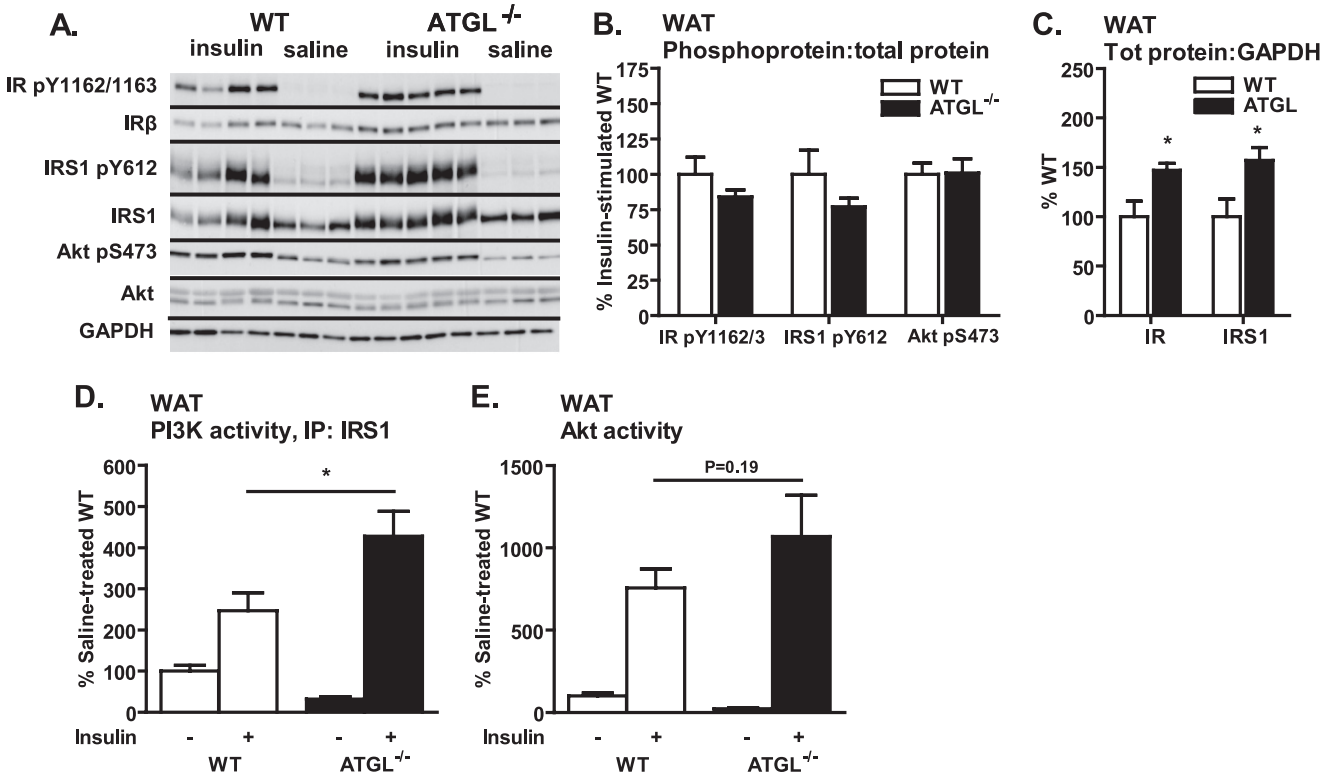

FIGURE 4. **WAT insulin signaling *in vivo*.** *A–E,* for insulin signaling in WAT *in vivo*, male mice at 10–12 weeks of age were fasted for 6 h, injected intraperitoneally with saline or insulin at 10 units/kg of body weight, and sacrificed 10 min thereafter. *A* and *B,* insulin-stimulated site-specific phosphorylation of IR, IRS1, and Akt as assessed by immunoblotting analysis ($n = 3–5$ per group). For quantification, phosphoproteins were normalized to the corresponding total proteins. GAPDH served as loading control. *A* and *C,* expression of total IR and IRS1 relative GAPDH control. *D,* IRS1-associated PI3K activity; and *E,* Akt activity ($n = 3–7$ per group). Data are expressed as mean ± S.E. *, $p < 0.05$ for effect of genotype as determined by unpaired two-tailed Student's *t* test (*B* and *C*) or one-way ANOVA (*D* and *E*).

although basal glucose uptake in skeletal muscle was enhanced *in vivo* (14), basal glucose transport was unchanged, and insulin-stimulated glucose transport was reduced in ATGL$^{-/-}$ mice *ex vivo* (Fig. 7*E*). Similar results were observed for EDL (data not shown), indicating that differences between *in vivo* and *ex vivo* findings are not likely because of differences in muscle fiber-type composition or fiber-type specific expression of ATGL. Taken together, these data suggest that tissue-specific as well as systemic effects influence glucose homeostasis and insulin action in skeletal muscle of ATGL$^{-/-}$ mice.

Local and Systemic Factors May Contribute to the Dissociation of in Vivo and ex Vivo Insulin Action in Skeletal Muscle of ATGL$^{-/-}$ Mice—To further explore the mechanisms underlying the differences between *in vivo* and *ex vivo* insulin action in skeletal muscle of ATGL$^{-/-}$ mice, we evaluated the role of both local and systemic factors in this phenotype. With regard to local factors, we characterized the intramyocellular lipid phenotype of ATGL$^{-/-}$ mice. As expected, intramyocellular TAG concentrations were substantially increased in ATGL$^{-/-}$ mice as demonstrated by Oil Red O staining of neutral lipid within skeletal muscle fibers (Fig. 8*A*) and using biochemical methods (Fig. 8*B*). However, although the absence of ATGL-mediated TAG hydrolysis would be expected to reduce other lipid metabolites, DAG concentrations were surprisingly increased (Fig. 8*C*). In contrast, ceramides were unchanged in ATGL$^{-/-}$ mice (Fig. 8*D*), and both total and species-specific long chain FA-CoAs were reduced in ATGL$^{-/-}$ mice with the exception of palmitoyl-CoA, which was unchanged (Fig. 8*E*). Because DAGs have been implicated in skeletal muscle insulin resistance, we evaluated possible mechanisms for their elevation by performing gene expression analysis of enzymes involved in their synthesis (glycerol-3-phosphate acyltransferase (GPAT1)), acylation (diacylglycerol acyltransferases 1 and 2 (DGAT1 and DGAT2, respectively)), and/or hydrolysis (hormone-sensitive lipase (HSL)). Compared with expression in WT mice, GPAT1 and DGAT2 were reduced, whereas HSL and DGAT1 were unchanged in ATGL$^{-/-}$ mice (Fig. 8*F*). These data suggest that reduced DGAT2-mediated acylation of DAG to TAG and/or an impaired compensatory increase in HSL-mediated DAG hydrolysis may contribute to increased DAGs in ATGL$^{-/-}$ mice.

With regard to systemic factors, we characterized the levels of circulating factors known to effect glucose homeostasis and insulin sensitivity (*i.e.* adipokines). RBP4, a proposed mediator of skeletal muscle insulin resistance, was decreased in serum of ATGL$^{-/-}$ mice (Fig. 8*G*). In contrast, serum resistin and adiponectin were unchanged between genotypes (data not shown). Thus, in addition to reduced serum NEFAs, reduced RBP4 may contribute to increased *in vivo* insulin action in skeletal muscle of ATGL$^{-/-}$ mice.

DISCUSSION

Intracellular TAG accumulation in insulin target tissues is generally associated with impaired insulin signaling leading to

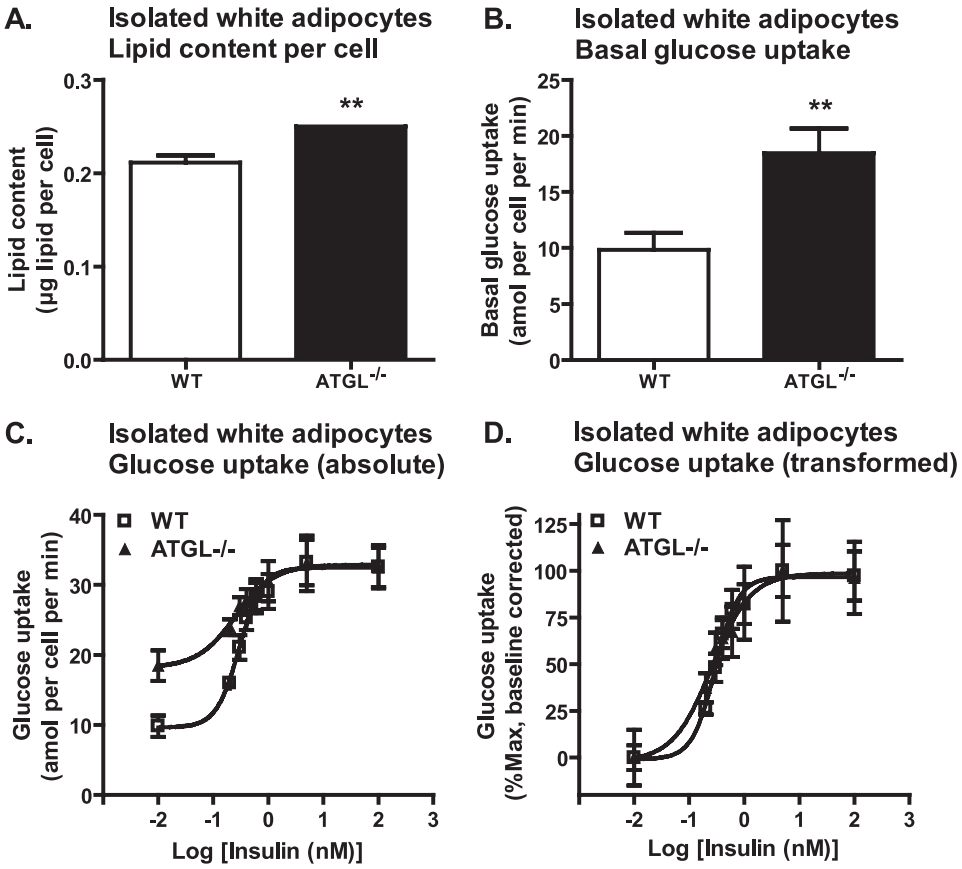

FIGURE 5. **Glucose transport in isolated white adipocytes.** For glucose transport into isolated adipocytes *ex vivo*, adipocytes were isolated from perigonadal WAT of 6- to 8-week-old male mice following a 6-h fast (n = 3–8 per group) and then assayed for uptake of [U-^{14}C]glucose in the presence of 0, 0.2, 0.3, 0.4, 0.6, 1, 5, or 100 nM insulin. *A,* lipid content per adipocyte. *B,* basal glucose transport in the absence of insulin. *C,* absolute values for the effect of insulin on glucose transport. *D,* transformed values for the effect of insulin on glucose transport after correcting for differences in basal glucose transport. Data are expressed as mean ± S.E. Curves were generated by nonlinear regression with no constraints (*C* and *D*). **, $p < 0.01$ for effect of genotype as determined by unpaired two-tailed Student's *t* test (*A* and *B*).

insulin resistance and overt diabetes. However, the paradoxical association of intramyocellular TAGs with insulin sensitivity in endurance-trained athletes challenges the notion that TAG accumulation *per se* is causal in this process (5). Thus, the mechanisms by which intracellular TAG accumulation affects tissue insulin action and the role of ATGL-mediated TAG metabolism in this process remain unclear. Mice with global targeted deletion of ATGL have improved glucose tolerance and insulin sensitivity despite increased adiposity and ectopic TAG accumulation in insulin target tissues such as liver and muscle. Thus, ATGL$^{-/-}$ mice represent a unique model to better understand the relationship between intracellular TAG metabolism and insulin resistance. Here we demonstrate that improved glucose tolerance and insulin sensitivity in ATGL$^{-/-}$ mice is not only due to reduced energy substrate availability but also due to tissue-specific changes in insulin action. We further demonstrate that skeletal muscle primarily contributes to improved whole-body insulin sensitivity in ATGL$^{-/-}$ mice and that both local and systemic factors influence tissue-specific insulin action in the setting of ATGL deficiency.

ATGL$^{-/-}$ mice on a pure C57BL/6 background demonstrate enhanced glucose tolerance and insulin sensitivity despite increased adiposity in accordance with previous findings in mice on a mixed genetic background (14). Both insulin-independent and -dependent mechanisms may contribute to this phenotype. In support of the former, glucose disposal is enhanced in ATGL$^{-/-}$ mice following a glucose challenge despite the absence of a concurrent insulin secretory response. The reduced availability of serum lipid substrates in ATGL$^{-/-}$ mice, even in the *ad libitum* fed state, likely enhances reliance on glucose as energy substrate as supported by an increased respiratory quotient and accelerated depletion of tissue glycogen and serum glucose during fasting and exercise (14, 28). This depletion of lipid and glucose substrate may also impair counter-regulatory responses to hypoglycemia. Previous studies demonstrating enhanced *in vivo* 2-[^{3}H]deoxyglucose uptake in muscle and liver support a role for these tissues in non-insulin-mediated glucose disposal in ATGL$^{-/-}$ mice (14). Our data in isolated adipocytes *ex vivo* further suggest that adipose tissue contributes to this process as well. Interestingly, the dramatic impairment in insulin secretion in ATGL$^{-/-}$ mice additionally implicates ATGL in glucose-stimulated insulin secretion from pancreatic beta cells. Indeed, Peyot *et al.* (29) have recently shown that ATGL is highly expressed in beta cells where it mediates TAG hydrolysis and influences fuel- and non-fuel-stimulated insulin secretion both *in vitro* and *in vivo*. Furthermore, biochemical data demonstrating increased TAG content in pancreas (14) and isolated islets (29) derived from ATGL$^{-/-}$ mice suggest that primary alterations in the islet lipid phenotype contribute to the observed impairments in beta cell function. Thus, ATGL$^{-/-}$ mice exhibit both enhanced non-insulin-mediated glucose disposal and impaired glucose-stimulated insulin secretion.

Although it is clear that ATGL$^{-/-}$ mice have improved glucose tolerance, the effect of ATGL deficiency on insulin sensitivity is more complex, likely involving competing mechanisms with dichotomous effects in different tissues. Whole-body insulin sensitivity is determined by the net effect of insulin action in insulin target tissues such as adipose tissue, liver, and skeletal muscle. Importantly, the effect of a given metabolic milieu on insulin action and vice versa can be very different for each of these tissues (30–32). This is clearly true in ATGL$^{-/-}$ mice in which insulin signaling *in vivo* is increased in skeletal muscle, unchanged or possibly increased in WAT, and decreased in BAT and liver. These data indicate that enhanced insulin signaling in skeletal muscle, rather than other tissues, is

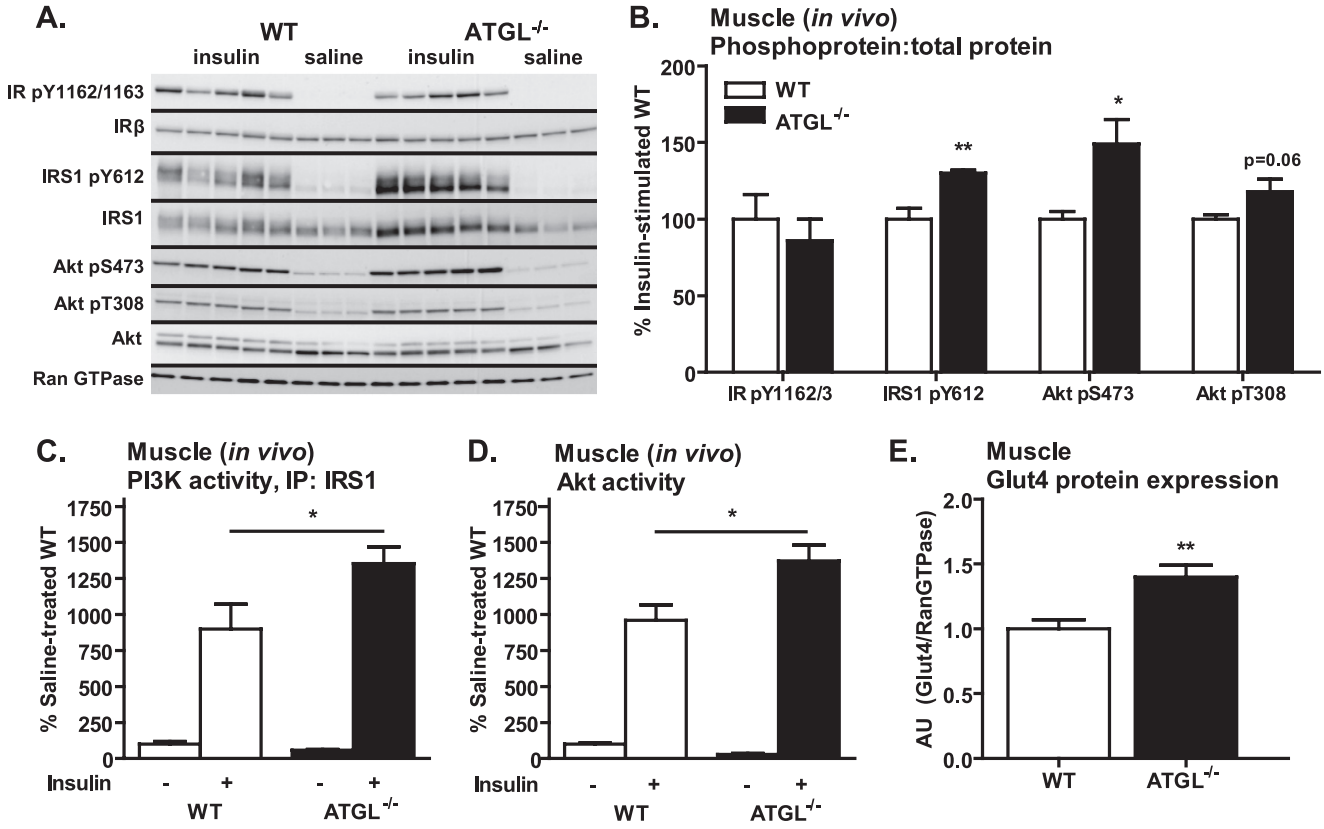

FIGURE 6. **Skeletal muscle insulin signaling *in vivo*.** Male mice at 10–12 weeks of age were fasted for 6 h, injected intraperitoneally with saline or insulin at 10 units/kg of body weight, and sacrificed 10 min thereafter. *A* and *B,* insulin-stimulated site-specific phosphorylation of the IR, IRS1, and Akt as assessed by immunoblotting analysis ($n = 3$–5 per group). For quantification, phosphoproteins were normalized to total proteins. Ran GTPase served as loading control. *C,* IRS1-associated PI3K activity, and *D,* Akt activity ($n = 3$–7 per group). *E,* Glut4 protein expression relative to Ran GTPase control as determined by Western blot analysis. Data from gastrocnemius muscle are shown. Data are expressed as mean ± S.E. *, $p < 0.05$; **, $p < 0.01$ for effect of genotype as determined by unpaired two-tailed Student's *t* test (*B* and *E*) or one-way ANOVA (*C* and *D*).

the primary contributor to whole-body insulin sensitivity in ATGL$^{-/-}$ mice. Potential mechanisms contributing to the observed tissue-specific changes in insulin action include the physiological response to reduced energy substrate availability, primary tissue-specific effects resulting from reduced ATGL-mediated TAG hydrolysis (*i.e.* changes in the intracellular lipid phenotype), or secondary systemic effects resulting from tissue-specific responses to the above (*i.e.* release of circulating factors such as adipokines or lipids themselves).

The interaction of these factors is most clearly exemplified by the effect of global ATGL deficiency on insulin action in skeletal muscle. Skeletal muscle is the primary site for insulin-mediated glucose disposal. Intramyocellular TAG accumulation is frequently associated with impairment of this process (*i.e.* insulin resistance) (33). Using both histological and biochemical methods, we confirm that TAGs indeed accumulate within skeletal muscle in ATGL$^{-/-}$ mice. Despite this intramyocellular TAG accumulation, *in vivo* insulin signaling is enhanced in skeletal muscle of ATGL$^{-/-}$ mice as indicated by increased phosphorylation of signaling molecules downstream of the IR (IRS1 and Akt), increased activity of PI3K and Akt, as well as increased expression of Glut4 protein. These findings are even more impressive in the context of relative energy substrate deficiency, which should favor peripheral insulin resistance to preserve glucose for vital organs. Interestingly, these changes in skeletal muscle insulin signaling disappear (or are even reversed in the case of Akt serine phosphorylation) under *ex vivo* conditions. Moreover, although basal glucose uptake into skeletal muscle is increased *in vivo* (14), basal glucose transport is unchanged, and insulin-stimulated glucose transport is decreased in ATGL$^{-/-}$ mice *ex vivo*. These differences in *in vivo versus ex vivo* results are not likely to be due to differences in muscle fiber-type composition or fiber-type specific expression of ATGL because ATGL expression was comparable in all muscles examined, and *ex vivo* findings were similar in muscles of divergent fiber types. These data have two important implications as follows: 1) primary effects of ATGL deficiency on intramyocellular lipid metabolism can negatively influence insulin action and decrease glucose transport into skeletal muscle; and 2) secondary systemic effects mediate the observed *in vivo* effects of ATGL deficiency on insulin action in skeletal muscle and are sufficient to overcome the primary local effects.

ATGL deficiency has several primary local effects on skeletal muscle lipid metabolism that may influence insulin action in that tissue. Importantly, ATGL deficiency results in dramatic intramyocellular TAG accumulation, even in the setting of reduced systemic FA delivery, consistent with a critical role for ATGL in intramyocellular TAG hydrolysis. Reduced TAG hydrolysis and FA delivery would also be expected to decrease (or at least not increase) other lipid metabolites, as is observed for FA-CoAs and ceramides. Interestingly, DAGs are unexpectedly increased in skeletal muscle of ATGL$^{-/-}$ mice. It is worth

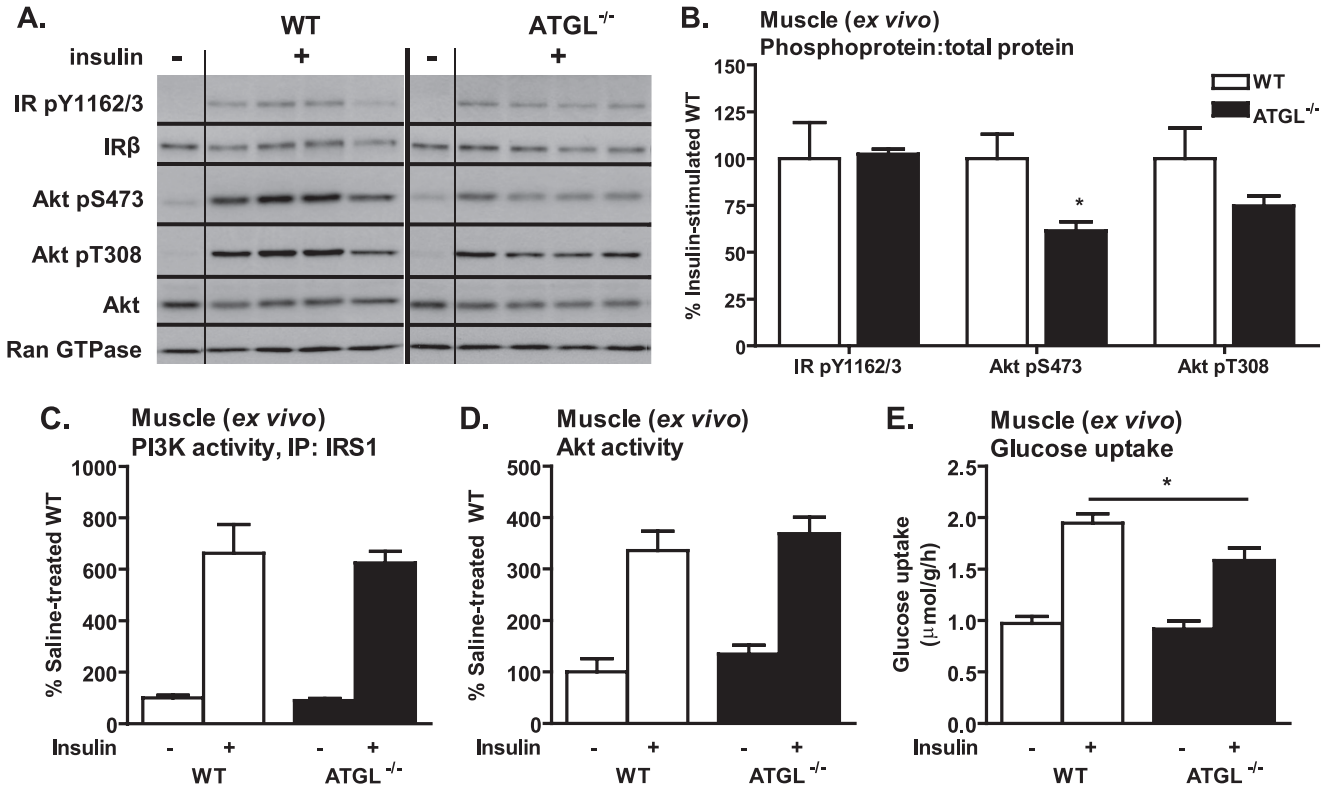

FIGURE 7. **Skeletal muscle insulin signaling and glucose transport *ex vivo*.** *A–D,* for analysis of insulin signaling in skeletal muscle *ex vivo*, soleus muscles were dissected from 6- to 10-week-old female mice following a 6-h fast and incubated in the presence or absence of 33 nM insulin. *A* and *B,* insulin-stimulated site-specific phosphorylation of the IR, IRS1, and Akt as assessed by immunoblotting analysis ($n = 3–5$ per group). For quantification, phosphoproteins were normalized to total proteins. Ran GTPase served as loading control. *C,* IRS1-associated PI3K activity; and *D,* Akt activity ($n = 3–9$ per group). *E,* for analysis of glucose uptake into skeletal muscle *ex vivo*, soleus muscles were dissected from 9- to 13-week-old female mice following a 6-h fast ($n = 9–11$ per group) and assayed for uptake of 2-[^{3}H]deoxyglucose in presence or absence of 33 nM insulin. Similar results were observed for EDL. Data are expressed as mean ± S.E. *, $p < 0.05$ for effect of genotype as determined by unpaired two-tailed Student's *t* test (*B*) or one-way ANOVA (*C–E*).

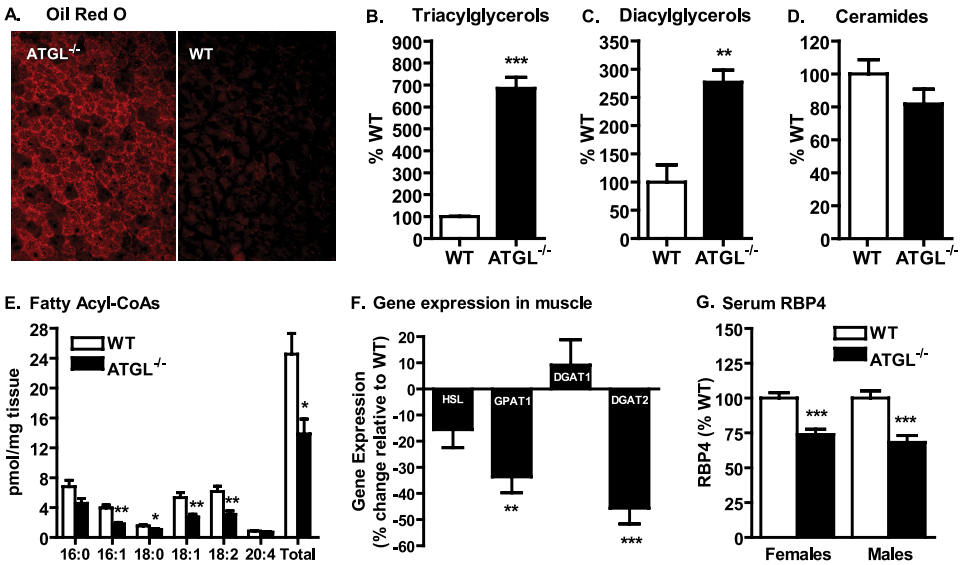

FIGURE 8. **Local and systemic factors contributing to skeletal muscle insulin action.** Lipid analysis was performed in skeletal muscle of 7–9-week-old mice following a 6-h fast. *A,* Oil Red O staining for neutral lipids in gastrocnemius of ATGL$^{-/-}$ and WT mice. *B,* TAG concentrations in soleus muscle of female mice ($n = 4$ per group). *C,* DAG; and *D,* ceramide contents in soleus muscle of mice of mixed gender ($n = 3–5$ per group). *E,* long chain FA-CoA concentrations in soleus muscle of male mice ($n = 6$). All lipid levels were normalized to tissue wet weight. *F,* gene expression analysis in skeletal muscle of 8-week-old female mice following a 6-h fast ($n = 8–12$). *G,* serum RBP4 in 7–10-week-old mice following a 6-h fast (8–16 per group) determined by immunoblot analysis. Data are expressed as mean ± S.E. *, $p < 0.05$; **, $p < 0.01$; ***, $p < 0.001$ for effect of genotype as determined by unpaired two-tailed Student's *t* test.

noting that skeletal muscle-specific transgenic overexpression of DGAT2, which increases TAGs and concomitantly decreases DAGs, promotes insulin resistance (34). In contrast, skeletal muscle-specific transgenic overexpression of DGAT1, which also increases TAGs and decreases DAGs, promotes insulin sensitivity (4). In addition, global deletion of HSL results in accumulation of intramyocellular DAGs but not TAGs (35–37). Thus, different enzymes involved in TAG metabolism can have very different effects on skeletal muscle insulin action despite similar effects on intracellular TAG content. These data support the notion that ATGL deficiency produces additional cellular changes independent of its effect on TAG content *per se* that may influence insulin action. Our data further suggest that inhibition of DGAT2-mediated acylation of DAGs and/or an impaired com-

pensatory increase in HSL-mediated DAG hydrolysis may contribute to this increase in DAGs in ATGL$^{-/-}$ mice. As yet, however, very little is known about the relationship between ATGL, HSL, and other enzymes contributing to lipolysis in skeletal muscle. Likewise, an increasing number of proteins such as the ATGL co-activator protein, CGI-58 (38), and lipid droplet proteins of the PAT family (named after perilipin, adipophilin, and TIP47 (tail-interacting protein of 47 kDa)) have been shown to interact with ATGL in adipocytes (39), but their role in skeletal muscle TAG metabolism and insulin action remains unclear. Unlike TAGs, DAGs have been directly implicated in lipid-induced insulin resistance via activation of novel protein kinase C and subsequent protein kinase C-mediated inhibition of insulin-stimulated IRS1 tyrosine phosphorylation and PI3K activity (40). However, it has been suggested that the specific metabolic pathways contributing to cellular DAG content and/or the specific subtypes of DAGs present also influence the overall effect of DAGs on insulin sensitivity (40). Thus, it remains unclear whether increased TAGs, DAGs, DAG subtypes, or a combination of these factors underlie the reduced *ex vivo* glucose transport in skeletal muscle of ATGL$^{-/-}$ mice.

In addition to the above local effects, global ATGL deficiency produces systemic effects that secondarily influence tissue-specific insulin action. As noted above, the presence of increased insulin signaling in skeletal muscle *in vivo* but not *ex vivo* implicates circulating factors in these effects. Evaluation of circulating factors known to influence insulin sensitivity revealed a decrease in serum RBP4 but no changes in adiponectin or resistin in ATGL$^{-/-}$ mice. RBP4 is an adipokine that has been linked to insulin resistance (41). Experimental conditions that increase RBP4 promote insulin resistance, whereas conditions that reduce RBP4 (*i.e.* genetic deletion) enhance insulin sensitivity (17). Thus, a reduction in RBP4 may contribute to the enhanced *in vivo* insulin action in skeletal muscle of ATGL$^{-/-}$ mice. In addition, chronically decreased levels of serum NEFAs or other lipids may themselves positively influence skeletal muscle *in vivo* insulin action in ATGL$^{-/-}$ mice by contributing to the reduction in intramyocellular FA-CoAs. Finally, we cannot rule out an effect of other systemic factors that have not yet been identified.

It is reasonable to assume that the above systemic effects result from tissue-specific changes induced by ATGL deficiency. Because adipokines potentially mediate these effects, it is worth noting that ATGL deficiency also has complex and unexpected consequences on insulin action in adipose tissue. Adipose tissue is the primary site for TAG storage and plays a crucial role in sensing the status of energy stores. Our data demonstrate that phosphorylation of insulin signaling molecules and Akt activity are unchanged, yet total expression of the IR and IRS1 as well as PI3K activity are increased in WAT *in vivo*. Thus, insulin action is unchanged or possibly even increased in WAT of ATGL$^{-/-}$ mice *in vivo*. The absence of any difference in insulin sensitivity (ED_{50}) or insulin responsiveness (V_{max}) in adipocytes *ex vivo* suggests that a positive effect of ATGL deficiency on insulin action is not significant *ex vivo*. In contrast, basal glucose transport is clearly increased in adipocytes. It has been shown that non-insulin-mediated glucose transport is proportional to adipocyte size (27); however, insulin-mediated glucose transport is generally *inversely* proportional to adipocyte size. Thus, the mere absence of insulin resistance in adipose tissue and isolated adipocytes of ATGL$^{-/-}$ mice, despite increased adiposity and adipocyte lipid content, is itself surprising. These data suggest that the ability of adipocytes to accurately assess the status of TAG stores is impaired in ATGL deficiency and that TAG accumulation in adipocytes is not necessarily detrimental to adipocyte insulin action.

Remarkably, in contrast to WAT, ATGL deficiency markedly impairs *in vivo* insulin signaling in BAT, the primary site of uncoupled lipid oxidation for thermogenesis. Specifically, phosphorylation of Akt and Akt activity are all decreased in BAT of ATGL$^{-/-}$ mice. Notably, BAT is one of the tissues most profoundly affected by TAG deposition because of ATGL deficiency, resulting in severely impaired thermogenesis and adaptation to cold (14). Interestingly, changes in *in vivo* insulin signaling in liver are virtually identical to those identified in BAT, suggesting a common underlying mechanism. Whether increased TAG accumulation *per se* or some other factor contributes to the *in vivo* insulin resistance in these tissues was not extensively evaluated in this study as they were for skeletal muscle above. Nevertheless, it is clear that neither BAT nor liver contribute to the enhanced insulin sensitivity of ATGL$^{-/-}$ mice.

In conclusion, these data suggest that ATGL deficiency leads to profound changes in the insulin signaling pathway that are distinct in different insulin target tissues. Specifically, insulin signaling *in vivo* is increased in skeletal muscle, unchanged or possibly increased in WAT, and decreased in BAT and liver. Thus, increased insulin action in skeletal muscle, rather than other insulin target tissues, primarily contributes to improved insulin sensitivity in ATGL$^{-/-}$ mice *in vivo*. Furthermore, differences in skeletal muscle insulin action *in vivo versus ex vivo* suggest that both local (tissue-specific) and systemic factors contribute to these effects. Importantly, ATGL deficiency produces additional cellular changes independent of its effect on TAG content *per se* that may influence lipid metabolism and insulin action. Further studies using animal models with tissue-specific alterations in ATGL are essential to further clarifying the specific role of ATGL in these fundamental metabolic processes. In addition, studies that explore the relationship between ATGL with other cellular proteins involved in intracellular TAG metabolism (*i.e.* HSL, CGI-58, and PAT family proteins) may provide critical insights into the mechanisms by which intracellular TAG metabolism contributes to glucose homeostasis and insulin action. These studies will be instrumental in promoting the understanding and treatment of lipotoxic metabolic disease.

REFERENCES

1. Schaffer, J. E. (2003) *Curr. Opin. Lipidol.* **14,** 281–287
2. Unger, R. H. (2003) *Endocrinology* **144,** 5159–5165
3. van Herpen, N. A., and Schrauwen-Hinderling, V. B. (2008) *Physiol. Behav.* **94,** 231–241
4. Liu, L., Zhang, Y., Chen, N., Shi, X., Tsang, B., and Yu, Y. H. (2007) *J. Clin. Invest.* **117,** 1679–1689
5. Goodpaster, B. H., He, J., Watkins, S., and Kelley, D. E. (2001) *J. Clin. Endocrinol. Metab.* **86,** 5755–5761

6. Shulman, G. I. (2000) *J. Clin. Invest.* **106,** 171–176
7. Summers, S. A. (2006) *Prog. Lipid Res.* **45,** 42–72
8. Lewis, G. F., Carpentier, A., Adeli, K., and Giacca, A. (2002) *Endocr. Rev.* **23,** 201–229
9. McGarry, J. D. (2002) *Diabetes* **51,** 7–18
10. Zimmermann, R., Strauss, J. G., Haemmerle, G., Schoiswohl, G., Birner-Gruenberger, R., Riederer, M., Lass, A., Neuberger, G., Eisenhaber, F., Hermetter, A., and Zechner, R. (2004) *Science* **306,** 1383–1386
11. Villena, J. A., Roy, S., Sarkadi-Nagy, E., Kim, K. H., and Sul, H. S. (2004) *J. Biol. Chem.* **279,** 47066–47075
12. Jenkins, C. M., Mancuso, D. J., Yan, W., Sims, H. F., Gibson, B., and Gross, R. W. (2004) *J. Biol. Chem.* **279,** 48968–48975
13. Kershaw, E. E., Hamm, J. K., Verhagen, L. A., Peroni, O., Katic, M., and Flier, J. S. (2006) *Diabetes* **55,** 148–157
14. Haemmerle, G., Lass, A., Zimmermann, R., Gorkiewicz, G., Meyer, C., Rozman, J., Heldmaier, G., Maier, R., Theussl, C., Eder, S., Kratky, D., Wagner, E. F., Klingenspor, M., Hoefler, G., and Zechner, R. (2006) *Science* **312,** 734–737
15. Kim, J. Y., van de Wall, E., Laplante, M., Azzara, A., Trujillo, M. E., Hofmann, S. M., Schraw, T., Durand, J. L., Li, H., Li, G., Jelicks, L. A., Mehler, M. F., Hui, D. Y., Deshaies, Y., Shulman, G. I., Schwartz, G. J., and Scherer, P. E. (2007) *J. Clin. Invest.* **117,** 2621–2637
16. Puri, V., Ranjit, S., Konda, S., Nicoloro, S. M., Straubhaar, J., Chawla, A., Chouinard, M., Lin, C., Burkart, A., Corvera, S., Perugini, R. A., and Czech, M. P. (2008) *Proc. Natl. Acad. Sci. U.S.A.* **105,** 7833–7838
17. Yang, Q., Graham, T. E., Mody, N., Preitner, F., Peroni, O. D., Zabolotny, J. M., Kotani, K., Quadro, L., and Kahn, B. B. (2005) *Nature* **436,** 356–362
18. Adamo, K. B., and Graham, T. E. (1998) *J. Appl. Physiol.* **84,** 908–913
19. Kim, Y. B., Nikoulina, S. E., Ciaraldi, T. P., Henry, R. R., and Kahn, B. B. (1999) *J. Clin. Invest.* **104,** 733–741
20. Zisman, A., Peroni, O. D., Abel, E. D., Michael, M. D., Mauvais-Jarvis, F., Lowell, B. B., Wojtaszewski, J. F., Hirshman, M. F., Virkamaki, A., Goodyear, L. J., Kahn, C. R., and Kahn, B. B. (2000) *Nat. Med.* **6,** 924–928
21. Tozzo, E., Gnudi, L., and Kahn, B. B. (1997) *Endocrinology* **138,** 1604–1611
22. Cushman, S. W., and Salans, L. B. (1978) *J. Lipid Res.* **19,** 269–273
23. Koopman, R., Schaart, G., and Hesselink, M. K. (2001) *Histochem. Cell Biol.* **116,** 63–68
24. Folch, J., Lees, M., and Sloane Stanley, G. H. (1957) *J. Biol. Chem.* **226,** 497–509
25. Guan, X. L., and Wenk, M. R. (2006) *Yeast* **23,** 465–477
26. Magnes, C., Suppan, M., Pieber, T. R., Moustafa, T., Trauner, M., Haemmerle, G., and Sinner, F. M. (2008) *Anal. Chem.* **80,** 5736–5742
27. Czech, M. P. (1976) *J. Clin. Invest.* **57,** 1523–1532
28. Huijsman, E., van de Par, C., Economou, C., van der Poel, C., Lynch, G. S., Schoiswohl, G., Haemmerle, G., Zechner, R., and Watt, M. J. (2009) *Am. J. Physiol. Endocrinol. Metab.* **297,** E505–E513
29. Peyot, M. L., Guay, C., Latour, M. G., Lamontagne, J., Lussier, R., Pineda, M., Ruderman, N. B., Haemmerle, G., Zechner, R., Joly, E., Madiraju, S. R., Poitout, V., and Prentki, M. (2009) *J. Biol. Chem.* **284,** 16848–16859
30. Koopmans, S. J., Maassen, J. A., Sips, H. C., Radder, J. K., and Krans, H. M. (1995) *Metab. Clin. Exp.* **44,** 291–297
31. Minokoshi, Y., Kahn, C. R., and Kahn, B. B. (2003) *J. Biol. Chem.* **278,** 33609–33612
32. Kahn, C. R., Brüning, J. C., Michael, M. D., and Kulkarni, R. N. (2000) *J. Pediatr. Endocrinol. Metab.* **13,** 1377–1384
33. Machann, J., Häring, H., Schick, F., and Stumvoll, M. (2004) *Diabetes Obes. Metab.* **6,** 239–248
34. Levin, M. C., Monetti, M., Watt, M. J., Sajan, M. P., Stevens, R. D., Bain, J. R., Newgard, C. B., Farese, R. V., Sr., and Farese, R. V., Jr. (2007) *Am. J. Physiol. Endocrinol. Metab.* **293,** E1772–E1781
35. Haemmerle, G., Zimmermann, R., Hayn, M., Theussl, C., Waeg, G., Wagner, E., Sattler, W., Magin, T. M., Wagner, E. F., and Zechner, R. (2002) *J. Biol. Chem.* **277,** 4806–4815
36. Voshol, P. J., Haemmerle, G., Ouwens, D. M., Zimmermann, R., Zechner, R., Teusink, B., Maassen, J. A., Havekes, L. M., and Romijn, J. A. (2003) *Endocrinology* **144,** 3456–3462
37. Park, S. Y., Kim, H. J., Wang, S., Higashimori, T., Dong, J., Kim, Y. J., Cline, G., Li, H., Prentki, M., Shulman, G. I., Mitchell, G. A., and Kim, J. K. (2005) *Am. J. Physiol. Endocrinol. Metab.* **289,** E30–E39
38. Lass, A., Zimmermann, R., Haemmerle, G., Riederer, M., Schoiswohl, G., Schweiger, M., Kienesberger, P., Strauss, J. G., Gorkiewicz, G., and Zechner, R. (2006) *Cell Metab.* **3,** 309–319
39. Granneman, J. G., Moore, H. P., Granneman, R. L., Greenberg, A. S., Obin, M. S., and Zhu, Z. (2007) *J. Biol. Chem.* **282,** 5726–5735
40. Timmers, S., Schrauwen, P., and de Vogel, J. (2008) *Physiol. Behav.* **94,** 242–251
41. Wolf, G. (2007) *Nutr. Rev.* **65,** 251–256